Netherlands Journal of Sea Research
21 (2): 79-94 (1987)

TEMPERATURE AND CURRENT FLUCTUATIONS DUE TO TIDAL ADVECTION OF A FRONT

J.J.M. VAN HAREN AND L.R.M. MAAS

Netherlands Institute for Sea Research, P.O. Box 59, 1790 AB Den Burg, Texel, the Netherlands

ABSTRACT

Records of current meters and thermistor chains moored at four closely spaced positions in the stratified Central North Sea during the summer of 1982 were analysed for "fluctuating signals" in the semidiurnal tidal band. The fluctuating current signal was defined as the residual time series after subtraction of a hindcast harmonic series (identified as barotropic currents) from the original data. The fluctuating temperature signal resulted after subtraction of the low-passed temperature field from the original data. During the period of interest a distinct frontal zone passed the moorings. Correlations and inspection of semidiurnal bandpass filtered graphs revealed no evidence for the existence of internal tides. Fluctuating temperature signals seemed to be caused mainly by rigid tidal advection of the frontal zone. The fluctuating current signals were partly caused by tidal advection of the geostrophic current, associated with the frontal zone, and partly by a phase shift in the barotropic current, due to stratification.

1. INTRODUCTION

Internal tide observations are among the most reported oceanographical phenomena in seas where stratification is present (SCHOTT, 1971; WUNSCH, 1975; HOLLOWAY, 1983; SHERWIN, 1987). Yet the identification of a temperature or baroclinic current fluctuation in the tidal frequency band with an internal tide is a step not to be taken without applying appropriate consistency tests (SCHOTT, 1977), since observed tidal band fluctuations may as well be created by barotropic tidal advection of low frequency current and temperature fields (MUIR, 1980; KOBLINSKY, 1981). These consistency tests are easily performed, as free (or damped) internal waves satisfy a number of dynamical relations among the measurable field variables as well as a dispersion relation. These relations are distinguishable from the relations governing tidal advection when three or more mooring stations are present (MUIR, 1980).

In this paper tidal band current and temperature time series are examined to test the existence of internal tide motions. A number of alternative processes is conjectured to explain observed phase relations of the dynamical variables. The observations carried out were performed during the summer of 1982, when the Royal Netherlands Meteorological Institute (KNMI), de Bilt, the Institute of Meteorology and Oceanography (IMOU), Utrecht, and the Netherlands Institute for Sea Research (NIOZ), Texel, cooperated to investigate the seasonal stratification in the Central North Sea. The measurement site has a relatively flat bottom at water depths of around 50 m. The site lies well on the continental shelf (Fig. 1). Data were obtained both from moored instruments, such as current meters and thermistor chains (Table 1), and from shipborne instruments, such as CTD and meteorological equipment.

All time series of measured current velocity components u (east) and v (north) are decomposed separately into three parts: (1) the tidal harmonic series $\vec{u_0} = (u_0, v_0)$, called barotropic currents, (2) the "fluctuating" (residual) velocity signals $\vec{u'} = (u', v')$, which resulted after subtraction of the barotropic series from the original time series, (3) the low-frequency field $\vec{u_g} = (\overline{U_g} \sin \alpha, \overline{U_g} \cos \alpha)$, with α denoting the direction of the field in degrees true North. Thermistor chain data were decomposed in a low frequency field $\overline{T}$ and in fluctuating temperature signals T', which can be regarded as variations on this low-

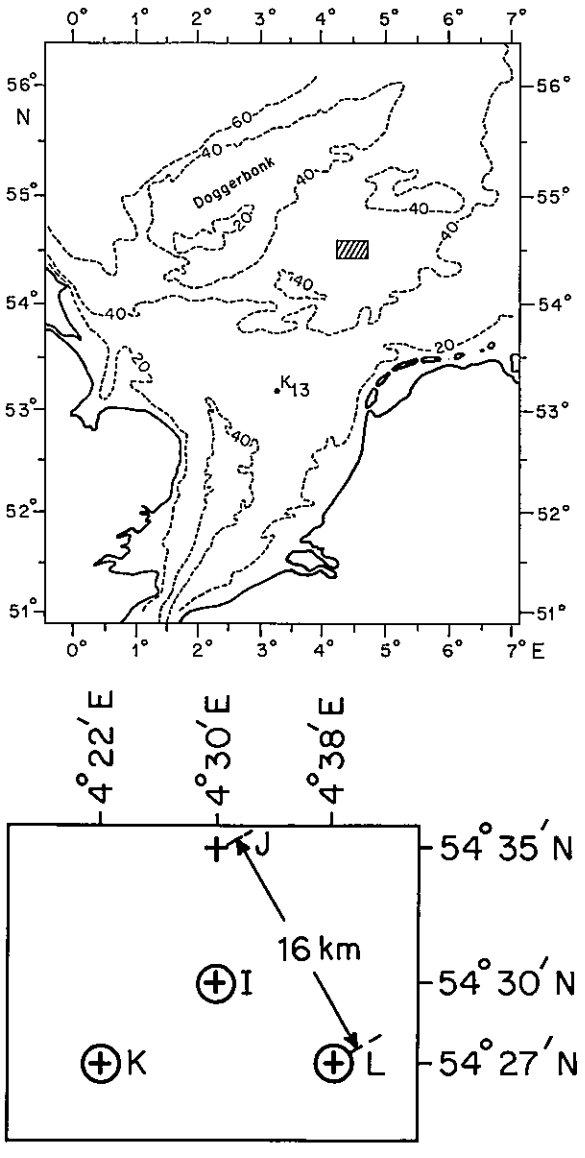

Fig. 1. a) Map of the North Sea with 20, 40, 60 m isobaths and position of mooring network in 1982 (the indicated rectangle). Wind observations are performed on platform K13. b) Current meter (+) and thermistor chain (O) mooring positions within the rectangle of a).

frequency field. The method of decomposition will be described in section 2.

During the analysed period (Table 1) the Central North Sea was stratified, the mean thermocline depth being 25 m (Fig. 2). Salinity did not contribute substantially to the observed density gradients. The south-eastern boundary to well-mixed waters was near the mooring positions (Fig. 3). After the passage of a (south-)westerly storm (Fig. 2c) around day 232, the wind-mixed layer deepened considerably (Fig. 2a), causing a steepening and intensification of this frontal zone (compare Figs 3a and 3b). The low-frequency current field at station I, shown in Fig. 2b, reveals a strong along-frontal jet around day 232, which is due to the frontal passage and not associated with the wind event, as its maximum occurs near the mean thermocline depth (VAN AKEN *et al.*, 1987). It is interesting to see how these low-frequent environmental conditions influence tidal band fluctuations. Therefore the description of the observations (section 3) and the discussion (section 4) will be focused on 3 time spans, which can be recognized in Fig. 2: the stratified period (days 215-230); the passage of the frontal zone (days 230-240); the "unstratified" period (from day 240 onward).

Acknowledgements.—This study was partly performed at the Institute of Meteorology and Oceanography, Utrecht, the Netherlands. The authors like to thank H.M. van Aken and G.J.F. van Heijst of this institute for the discussions about the interpretation of the data. Current meter data records were kindly supplied by H.W. Riepma of the Royal Netherlands Meteorological Institute, de Bilt. We thank captain Blok and his crew of R.V. "Tyro" for the pleasant cooperation during the hydrographic cruises, and C. Veth of the Netherlands Institute for Sea Research, Texel, who made the cruises possible by doing the bulk of the organizing work. We like to thank J.T.F. Zimmerman for critically reading the manuscript. The authors are supported by a grant of the Netherlands Organization for the Advancement of Pure Research (Z.W.O.).

2. DATA HANDLING

All data were analysed on a CYBER-computer. As we were interested in tidal motions the data were first turned into time series of hourly values by simple averaging. To obtain low-passed temperature (and velocity) signals, thermistor chain (and current meter) data were smoothed by using 50-hour running mean filters twice. The fluctuating temperature signal was computed by subtracting the low-passed temperature signal from the original data.

As we were interested in semidiurnal tidal band velocity signals related to stratification, such as internal tidal currents, these signals were isolated from the measurements. After in-

TABLE 1

Positions, depths, local sea depth, operational periods and sampling periods of current meters and thermistor chains in 1982. dt = sampling period. * Every 2 m a thermistor.

	N	*E*	*depths (m)*	*water depth (m)*	*period (year-day)*	*dt (min)*
Current meters						
I	54°30′	4°30′	12, 24, 30, 37	49	215-252	10
			18		215-239	10
			44		215-240	10
J	54°35′	4°30′	12, 43	48	215-252	10
K	54°27′	4°22′	12, 27, 44	49	215-252	10
L	54°27′	4°38′	12, 27, 42	47	215-252	10
Thermistor chains						
I	54°30′	4°30′	11-31*	49	215-253	15
K	54°27′	4°22′	11-31*	49	215-253	15
L	54°27′	4°38′	9-29*	47	215-253	15

spection of the amplitude spectrum of the original time series u, v, the harmonic tidal constituents ω_n : O_1, K_1, N_2, M_2, S_2, M_4 and M_6 were used in a harmonic analysis over the total span of time of at least one month (DRONKERS, 1964). As the barotropic tidal currents showed a vertical structure due to bottom friction (MAAS & VAN HAREN, 1987), it was considered necessary to define the harmonic series $u_0 = \sum_n u_0(\omega_n)$ at each mooring position and depth as the "barotropic current" record for that specific position and depth. The amplitudes and phases for the most energetic tidal constituent M_2 at 12 m depth are given in Table 2 as an example. The resulting signals u′, hereafter referred to as "fluctuating current" signals, are defined as $u' = u - \sum_n u_0(\omega_n)$ for each mooring position and depth. On the assumption that internal tides (and other modes of motion) are not phase locked to the barotropic currents over the analysed time span (HOLLOWAY, 1983), these are contained entirely in u′. All calculations were performed for both velocity components separately. From the normalized variances before and after performing harmonic analysis it was found that the barotropic currents contained 80-90% of the total energy in east velocities u and 25-80% in north velocities v.

Because of the broad semidiurnal frequency band, which contained most of the energy as can be seen in Fig. 4, the fluctuating signals were bandpass filtered. A symmetric cosine filter excluding the inertial frequency was used after tapering the time series with a similarly shaped window. Table 3 shows the half amplitude filter frequencies.

Besides inspection of the graphs of the fluctuating signals, numerous correlations between different time series were calculated to obtain phase relationships between the field variables. In order to increase the number of degrees of freedom, correlations performed for time spans of 64 hours were averaged. This length was chosen to obtain correlation results for the semidiurnal frequency band which had a width similar to the width of the bandpass filter (Table 3). The significant coherence level c was calculated according to THOMPSON (1979) as $c = \{1 - \alpha^{1/(n-1)}\}^{1/2}$, where n denotes the number of estimates and 1-α the confidence level, which was chosen as 95% . The minimal number of estimates ($n > 5$; THOMPSON, 1979) forced a lower boundary time-series length of nearly two weeks ($\cong 5 \times 64$ hours). To investigate the time evolution of the correlations, calculations were performed for these minimal time intervals of two weeks (Fig. 5). To obtain a slightly more detailed picture of the time evolution, consecutive calculations overlapped half way.

3. OBSERVATIONS AND CORRELATION RESULTS

Fig. 6 shows raw and bandpass filtered temperature fluctuations at station I. Other stations show similar pictures. Comparison of the raw

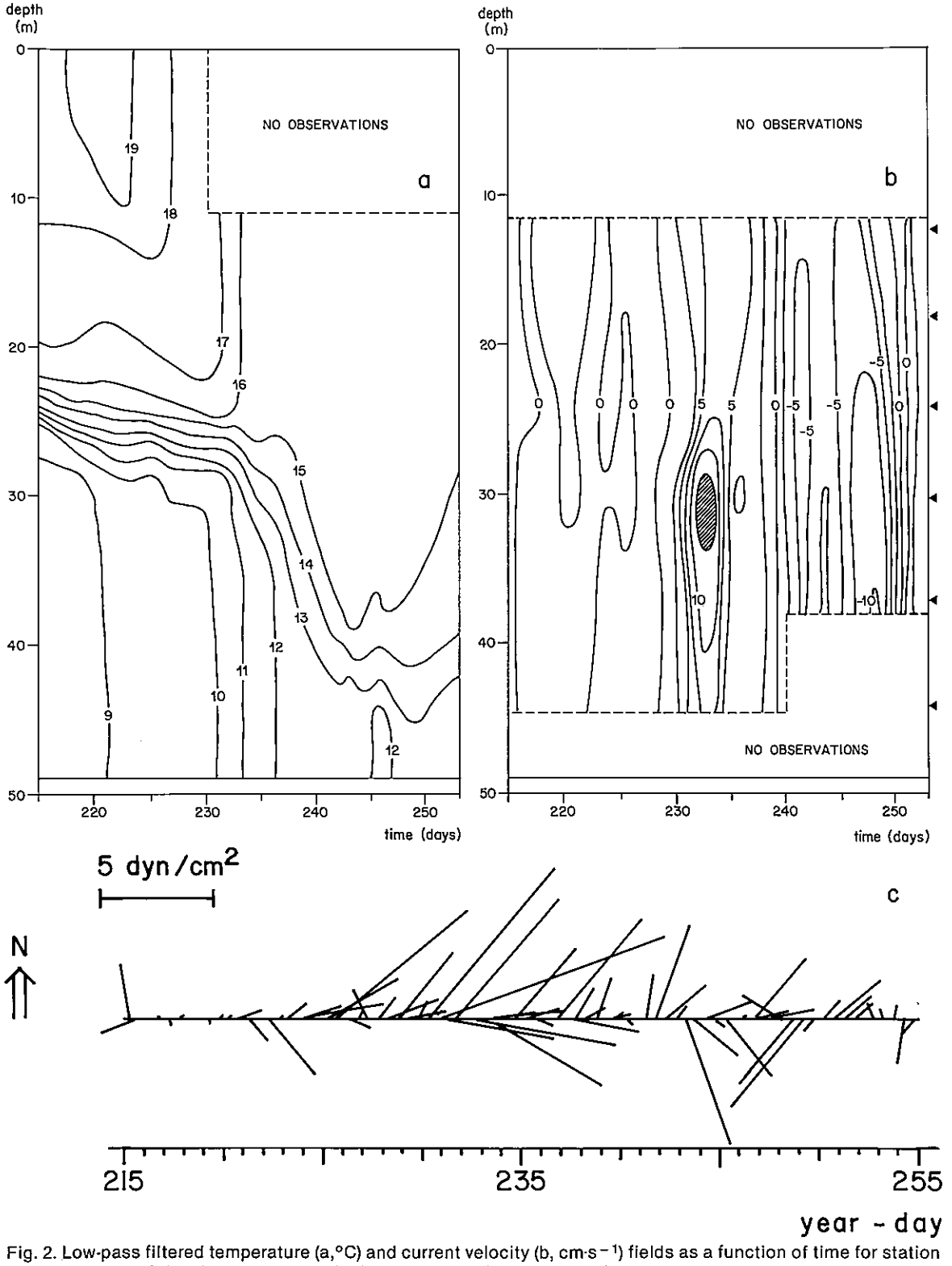

Fig. 2. Low-pass filtered temperature (a,°C) and current velocity (b, cm·s^{-1}) fields as a function of time for station I. The direction of the shown current velocity component is 33° true N (from VAN AKEN *et al.*, 1987). (c) Observed windstress at platform K13 (Fig. 1), depicted according the oceanographic convention (from MAAS & VAN HAREN, 1987).

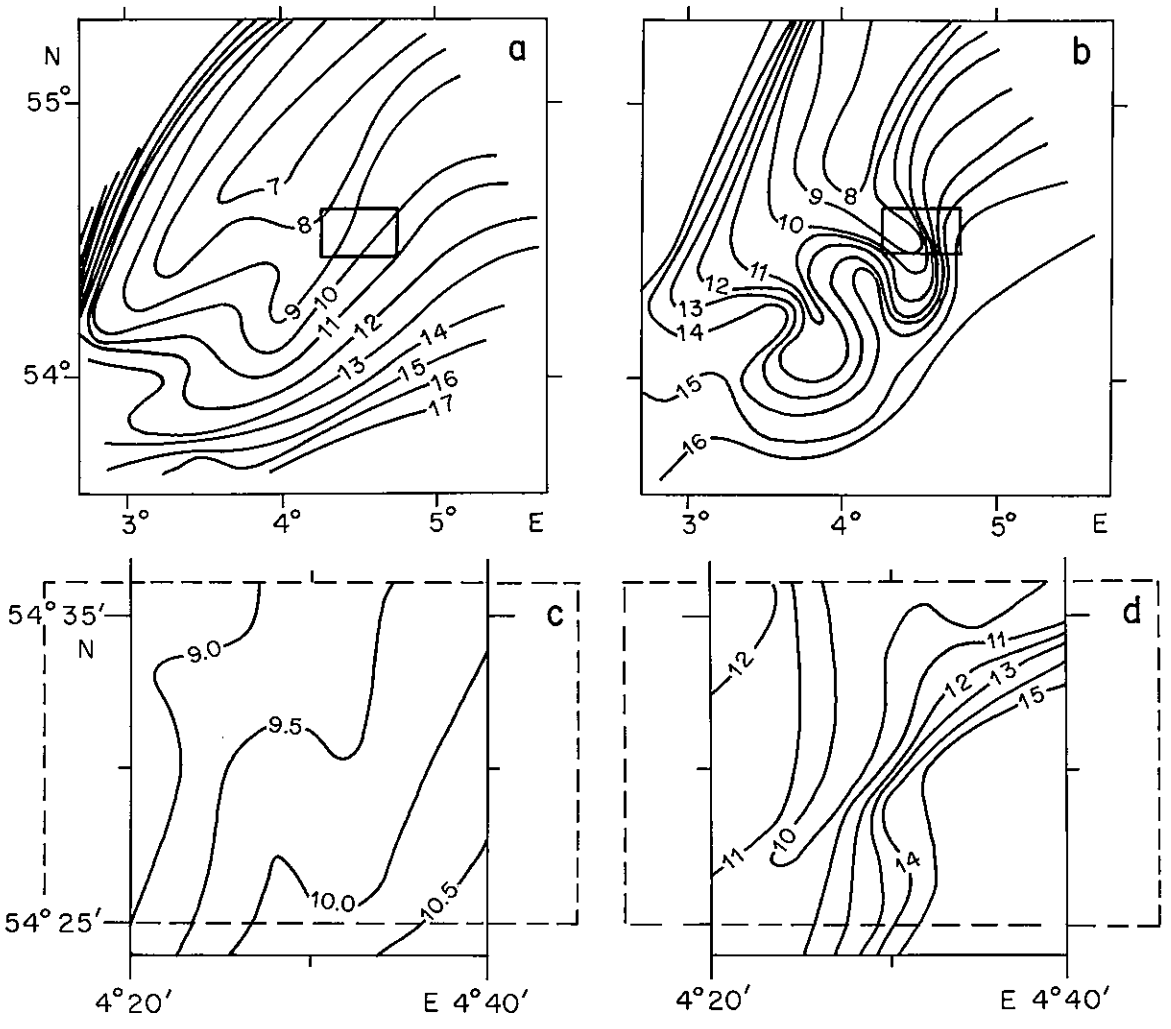

Fig. 3. Horizontal temperature distributions (°C) at 5 m from the bottom obtained during large-scale (station separation $\Delta x = 15$ km) hydrographic surveys on days 229 (17-8-1982) (a) and 260 (17-9-1982) (b), and during small-scale ($\Delta x = 4$ km) surveys on days 226 (14-8-1982) (c) and 269 (26-9-1982) (d). In all figures the rectangle refers to the one in Fig. 1. (after VAN AKEN, 1983).

TABLE 2

Amplitudes (cm·s^{-1}) and phases ϕ (degrees) from Harmonic Analysis for the tidal frequency M_2 of the east (u_0) and north (v_0) barotropic velocity components at 12 m depth. Phases with respect to 1-1-1982 24.00 GMT. Errors in the observed amplitudes and phases were estimated, by TEE's (1982) method, with an overall root-mean-square value of the fluctuating currents of: $\nu = 5$ cm·s^{-1}. This value implies an error of the harmonic amplitudes of $\Delta u_0 \cong \Delta v_0 = \sqrt{2}\nu M^{-1/2} \cong 0.4$ cm·s^{-1}, where M denotes half the number of hourly data points (typically M = 400, Table 1).

The error of the harmonic phases reads respectively, $\Delta\phi_{u_0} = \sin^{-1}(\Delta u_0/u_0) \cong 1^0$, $\Delta\phi_{v_0} = \sin^{-1}(\Delta u_0/v_0) \cong 15^0$.

station	u_0	ϕu_0	v_0	ϕv_0
I	23.6	5	.8	285
J	22.7	4	1.2	317
K	22.7	8	2.1	342
L	24.6	6	1.2	58

and bandpass filtered signals seems to show that relatively energetic supertidal frequency motions occur before day 230 (stratified period). Distinct semidiurnal tidal band temperature fluc-

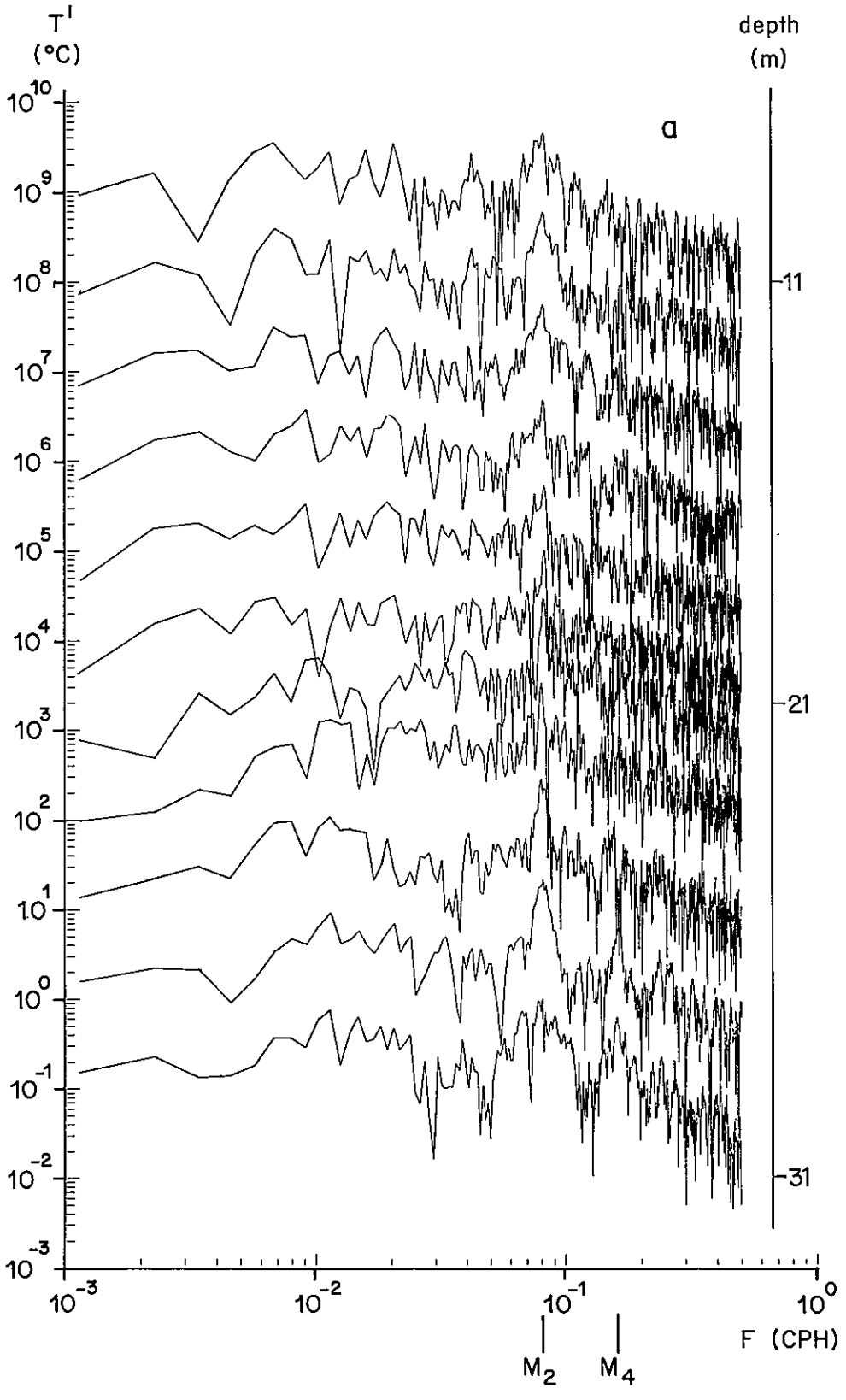
T'
(°C)
depth
(m)
a
10^{10}
10^{9}
10^{8}
10^{7}
10^{6}
10^{5}
10^{4}
10^{3}
10^{2}
10^{1}
10^{0}
10^{-1}
10^{-2}
10^{-3}
11
21
31
10^{-3}
10^{-2}
10^{-1}
10^{0}
F (CPH)
M_2
M_4

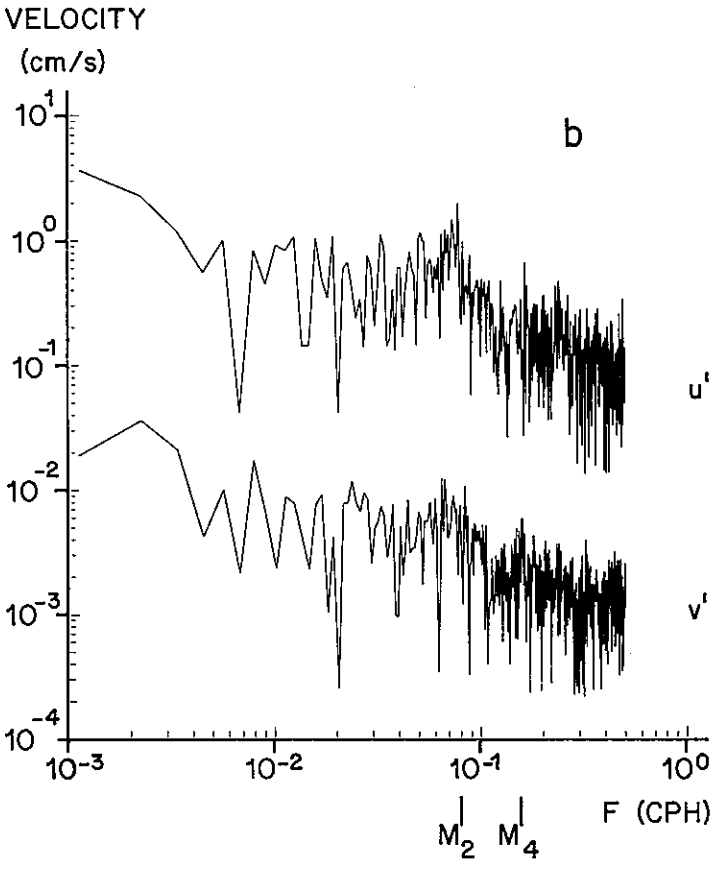

Fig. 4. Raw amplitude spectra of temperature fluctuations T' (a) and velocity fluctuations u', v' (b). Note that from 31 m upwards the T' spectra are shifted by a factor of 10 and that v' is multiplied by 10^{-2}.

TABLE 3

Half amplitude response frequencies (x 10^{-4} rad·s^{-1}) of bandpass filter (a) and correlation band (b). $M_2 = 1.405189 \times 10^{-4}$ rad·s$^{-1} \cong 5/64$ hr^{-1}.

	(a)	*(b)*
σleft	1.222	1.227
σright	1.571	1.500

tuations, occurring at the thermocline depth, are most pronounced between days 230 and 237, when the thermocline deepens (Figs 2a and 6).

The semidiurnal tidal band shows a slight amplitude increase for u' and v' at 30, 37 and 44

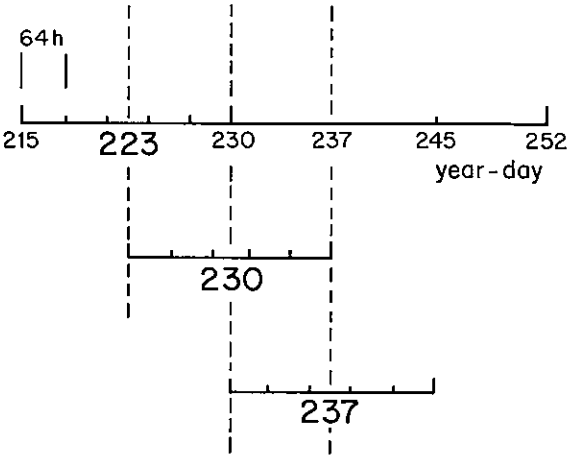

Fig. 5. Schematic of the division of total time series into smaller blocks of 64 hours each, intended for calculation of the correlation. Each calculation with 5 degrees of freedom (*i.e.* the average of five consecutive intervals of 64 hours) represents a time span of nearly 14 days centered around the enlarged year-day numbers. Consecutive correlations are shifted in time by 7 days.

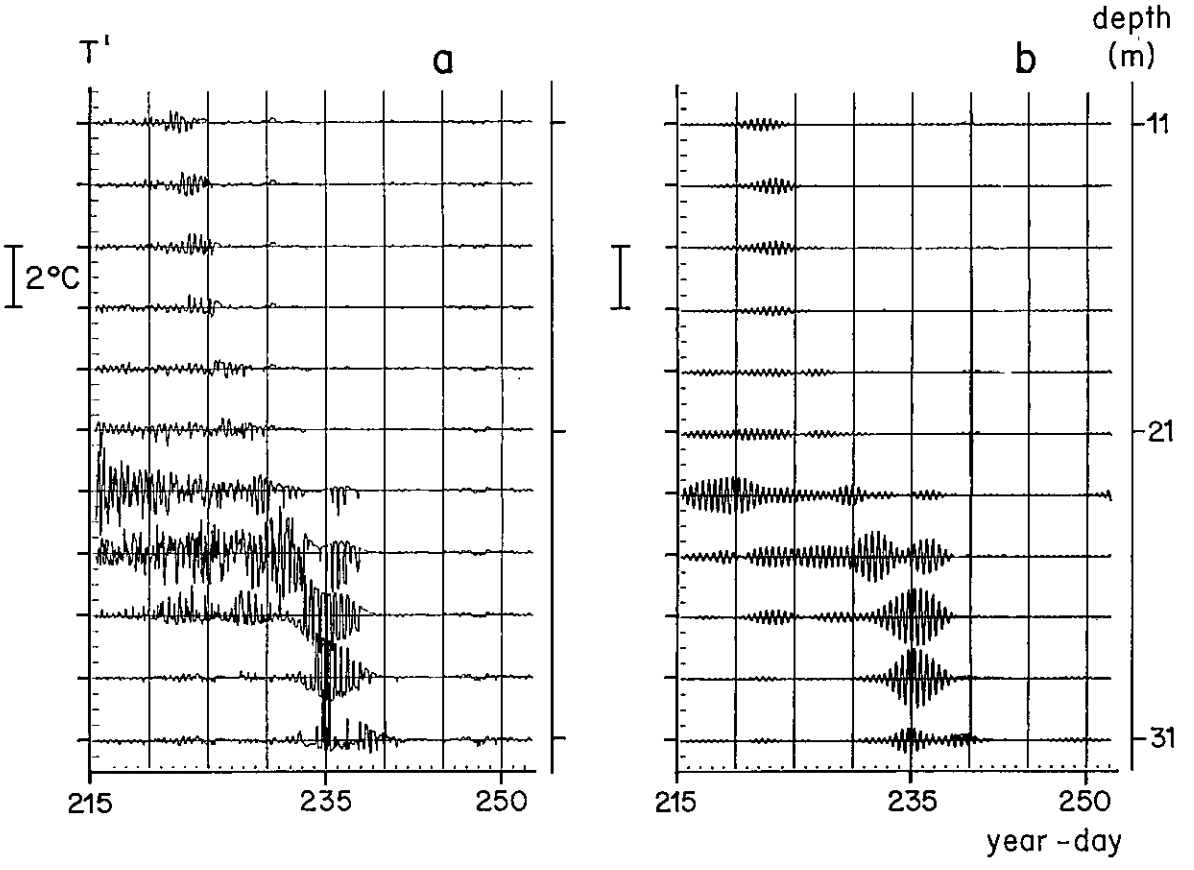

Fig. 6. Raw (a) and bandpass filtered (b) time series of fluctuating temperature signals T' (°C) for station I (from MAAS & VAN HAREN, 1986).

m depth at station I around day 233 (Fig. 7). The bandpass filtered signals seem to have an intermittence period of 4-5 days, while the overall amplitude ratio $|v'| / |u'| \cong 0.7$. Other stations show similar pictures and results.

About one fourth of all possible correlations between time series of u', v', T' and u_0 at different horizontal and vertical positions have been calculated. Phase differences between time series are shown in Table 4 only when the signals are correlated. Below the thermocline, u_0 at 30 m depth is correlated with T' in the stratified period and during the passage of the front (Table 4a). T' lags u_0 by 115°, at station I and by 140°, at station L (not shown; calculations performed with u_0 at 27 m). Correlation calculations between temperature fluctuations show hardly any coherence (Table 4b). The same might be said of correlations between u' and T' (Table 4c). Table 4d shows small phase differences of about 20° when correlation occurs between vertically separated u's. Other combinations of pairs u' at station I have also been calculated but are not shown in Table 4d as no coherence existed. The correlation in u' between different moorings is remarkably good (Table 4e). Phase differences are very small (~ 20°), but larger than the phase differences in the barotropic currents between the mooring positions (2-3°; Table. 2). Only from 30 m downwards some coherence between u' and u_0 exists (Table 4f). The phase difference of some 95° around day 237 was found at all stations at similar depths, although at no station the significant coherence level was exceeded. A phase difference of 75° dominates the results for correlation of u' and v' at the same depth (Table 4g).

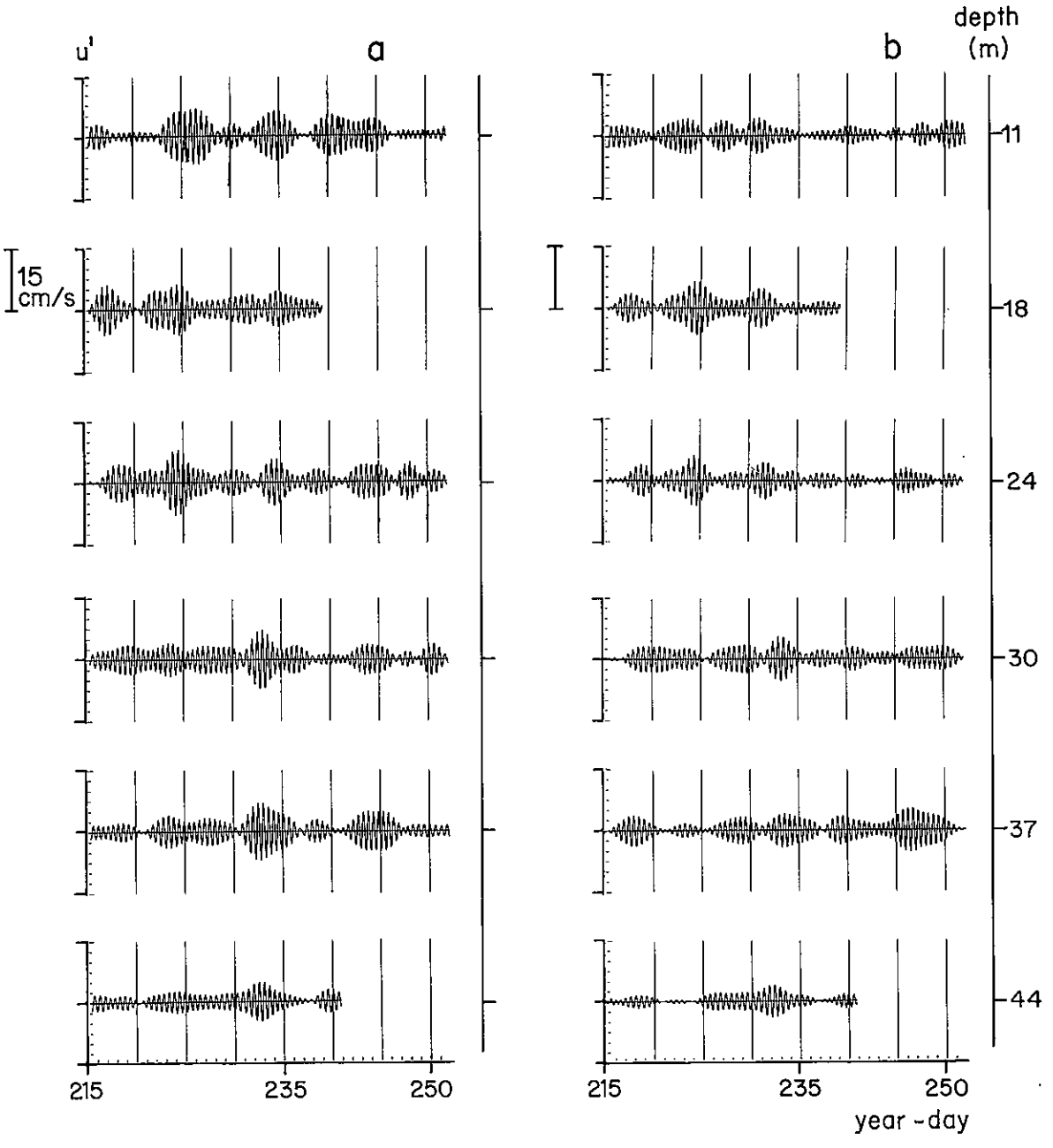

Fig. 7. Bandpass filtered time series of fluctuating velocity signals u' (a) and v' (b) for station I (from MAAS & VAN HAREN, 1986).

4. DISCUSSION

4.1. INTERNAL TIDES

Interaction of the barotropic tide with a local change in depth, such as Dogger Bank, can generate internal tides which propagate away on the thermocline (BAINES, 1982). Because of their nature the internal tides should be contained in the fluctuating signals. SCHOTT (1971) assigned Dogger Bank as the generation site for the internal tidal waves he detected. His moorings were

TABLE 4

Time evolution of phase differences in degrees between time series which correlate with 95% confidence. Positive phase difference in A*B denotes A lags B. The notation, when fully used, reads $A_{b,c}$ where A = correlated parameter, b = mooring station, c = depth of meter (m). When no phase difference is shown no coherence exists. (a) $u_{0_{l,30}}$*T_l'; (b) T_l'*T_K'; (c) $u_{l,30}$ *T_l'; (d) u_l'*u_l' in the vertical plane; (e) u'*u' in the horizontal plane (f) u_l'*u_{0_l}. Between brackets: points correlating at the 90% confidence level; (g) u_l'*v_l'. +: no results because of failure of current meters I18 and I44.

(a) Day: *Depth*	*223*	*230*	*237*	*245*	*(b) Day:* *Depth*	*223*	*230*	*237*	*245*
T'29			115		31		16		
T'27	−118	118	112		29				
T'25		135	114		27			178	
T'23	124				25				
T'21	127				23			59	
T'15	115				21	89		28	
(c) Day: *Depth*	*223*	*230*	*237*	*245*	*(d) Day:* *Depth*	*223*	*230*	*237*	*245*
T'29					12*24			−33	−24
T'27					24*30				17
T'25			−170		30*44		24		
					30*37	25	−2	−5	
					37*44	10	25	25	
(e) Day: *Depth*	*223*	*230*	*237*	*245*	*(f) Day:* *Depth*	*223*	*230*	*237*	*245*
I12*J12	−5	−8	−10	−10	12				
I12*K12	−20	−16	−3	−3	18			+	+
I12*L12	−13	−22	6	15	24				
J12*K12		−6	10	0	30	−41		(93)	
J12*L12	−3	−13	14	23	37	−81		(101)	
K12*L12		−6	14	21	44				+
I44*I43		19	6	+					
I44*K44	1	−2	−2	+					
I44*L42	−42	−25	−2	+					
J43*K44	11	15	−4	10					
J43*L42	−12	−8	−5	−2					
K44*L42	−38	−22	−2	−18					
(g) Day: *Depth*	*223*	*230*	*237*	*245*					
12									
18	76	77							
24	67	75	73						
30	97	77							
37		64		116					
44	157		69						

positioned at the same distance of about 110 km from Dogger Bank as ours, but in deeper water (82 m) to the north of it. In general, internal tidal wave lengths are larger in deeper water, which results in lower dissipation rates (MARTINSEN & WEBER, 1981). An estimation of the internal tidal wave length can be calculated from the dispersion relation governing free internal waves in a two-layer model with depths h_s and h_b for the surface and bottom layer (LEBLOND & MYSAK, 1978):

$$\lambda^2 = (2\pi)^2/(\sigma^2 - f^2)\cdot g\alpha\Delta T h_s h_b/(h_s + h_b)$$

where

g = acceleration of gravity (9.81 $m\cdot s^{-2}$)

α = thermal expansion coefficient

$(2{\cdot}10^{-4}(°C)^{-1})$
σ = semidiurnal tidal frequency
$(1.405 \times 10^{-4}$ rad·s$^{-1})$
f = inertial frequency
$(1.184 \times 10^{-4}$rad·s^{-1} at 54°30'N)
ΔT = temperature difference over the thermocline (°C)

Using values from Fig. 2a and Table 1 an internal tidal wave length of 32 km can be estimated, which is much smaller than the barotropic tidal wave length of O (10^3 km). Given the mooring separation distances (Fig. 1b) and the internal tidal wave length, horizontal phase differences in internal tidal signals in the order of 90°-180° between the moorings are to be expected, in contrast to a measured phase difference of 2°-3° for the surface tide (Table 2).

Since the mooring positions are situated far enough from the generation site (presumably Dogger Bank), internal tidal waves might be described as propagating free waves. Modelling the stratification by a two layer sea governed by the common equations describing long wave motions in an incompressible sea allows theoretical phase relationships between the physical parameters to be derived, describing a first mode (usually the most energetic mode) free internal wave at a single location, as given in Table 5. The phase relationships between the surface tidal current and the elevation and current field associated with the internal tidal wave depend on the distance from the generation site.

Although the thermocline was well pronounced at least during the first 14 days of measurement, hardly any evidence for the presence of internal tides was found from fluctuating current velocity or temperature observations. While bandpass filtered T' with amplitudes of 1.5°C during the stratified period are visible in Fig. 6 ,

TABLE 5

Local phase differences between parameters describing a theoretical first mode propagating free internal wave (s = surface, b = bottom). Positive phase difference denotes z lagging y.

Y:	T'	u'_s	u'_b	v'_s	v'_b
z					
T'	-				
u'	0°	-			
u'	180°	180°	-		
v'	−90°	−90°	−90°	-	
v'	90°	90°	90°	180°	-

correlations in the horizontal plane hardly occur and do not resemble an expected phase difference in the range of 90° to 180° (Table 4b). The same conclusion applies to the correlations in Table 4c between u' and T', since the expected phase difference is 180°. Although Table 4e shows a strong coherence for u' in the horizontal plane, no agreement is found between the calculated and theoretically expected phase differences, which apply for free internal tides. Also, as the observed phase relations might be due to a standing internal wave component, the corresponding theoretical phase relations are not confirmed either. The evidence for internal waves is thus absent.

The question then arises why internal tides cannot be found in our observations? First, the only reasonably possible generation site for internal waves, *i.e.* Dogger Bank, lies at a distance of 3.5 times the calculated internal tidal wavelength. Other investigators have found that internal waves (generated at a continental shelf edge) were extinguished after travelling on the continental shelf a distance of 2-3 wavelengths from their generation site (PETRIE, 1975; HOLLOWAY, 1983). Thus, free internal waves radiating away from Dogger Bank may have dissipated on arrival at our measurement site. In contrast, SCHOTT'S (1971) observed internal tidal wavelengths were larger, because he was measuring in deeper waters (82 m). Secondly, Figs 2a and 3 show a frontal zone close to the moorings. Fluctuating signals u' due to frontal advection or due to barotropic currents, shifted in phase at such a frontal zone, are likely to drown any remaining internal tidal signals, as will be shown in the next subsections.

4.2. FRONTAL ADVECTION

Due to the existence of a frontal zone close to and even passing the moorings, the fluctuating signals u' might as well be due to tidal advection of this front. However, some uncertainties about the distinction between signals due to tidal advection and due to internal tides exist in the literature. Although mentioning the possibility of frontal advection as a mechanism for their measured temperature fluctuations from a single mooring close to a shelf break front, JONES & PADMAN (1983) interpret their data in terms of internal tides exclusively. By using an estuarine model of the strongly stratified St. Lawrence estuary, MUIR (1980) demonstrates the effects of

frontal advection on the density profiles measured at a single mooring position. According to MUIR (1980) most of the measured density fluctuations are to be ascribed to frontal advection rather than to internal tides, although they are registrated in the same way. As MUIR (1980) rightly points out, in order to distinguish between internal tides and rigidly advected horizontal density gradients, one needs three or more horizontally spaced moored instruments. KOBLINSKY (1981) shows, using a simple model, that on the West Florida Shelf measured temperature fluctuations are due to frontal advection. He interpreted the absence of distinct peaks in the temperature frequency spectrum as an absence of internal tides. According to KOBLINSKY (1981) and assuming a stationary front, with $\partial \overline{T}/\partial x$ constant, a rectilinear tidal current $\vec{u_0} = (U_0 \cos\sigma t, 0)$ (Table 2), $\partial T'/\partial x << \partial \overline{T}/\partial x$ and $|u'| << U_0$, the time variation of the fluctuating temperature signal due to frontal advection is given by:

$$\partial T'/\partial t = -U_0 \cos\sigma t \cdot \partial \overline{T}/\partial x. \qquad (1)$$

A phase difference of 90° between u_0 and T' is to be expected when they are related according to (1). The amplitude of T' will depend on the ratio of the frontal width to the tidal excursion amplitude $L_e = U_0/\sigma$.

When the associated spatially varying horizontal pressure gradient (∇p) is geostrophically balanced according to:

$$\varrho f \hat{k} \times \vec{u_g} + \nabla p = 0,$$

where $\hat{k}$ denotes the vertical unit vector, we may similarly expect local current fluctuations due to rigid tidal advection of the density field (ϱ) and its associated geostrophic current $\vec{u_g}$. Thus at a moored position we may expect velocity fluctuations due to rigid tidal advection according to:

$$u'(x,t) = \vec{u_g}\,(x - L_e \sin\sigma t). \qquad (2)$$

Adopting a bell-shaped profile of the geostrophic current amplitude $\overline{U_g} = \hat{U}_g \cosh^{-2}(x/L_g)$ (Fig. 8a) with $x = 0$ at the jets maximum and L_g denoting the geostrophic current width, equation (2) predicts local velocity fluctuations. Fig. 8 shows some synthetic results for u', which depend, both in amplitude and in phase, on the distance of the mooring position relative to the jets' axis (x), and on the tidal excursion amplitude L_e, both in terms of L_g. For example, the second harmonic

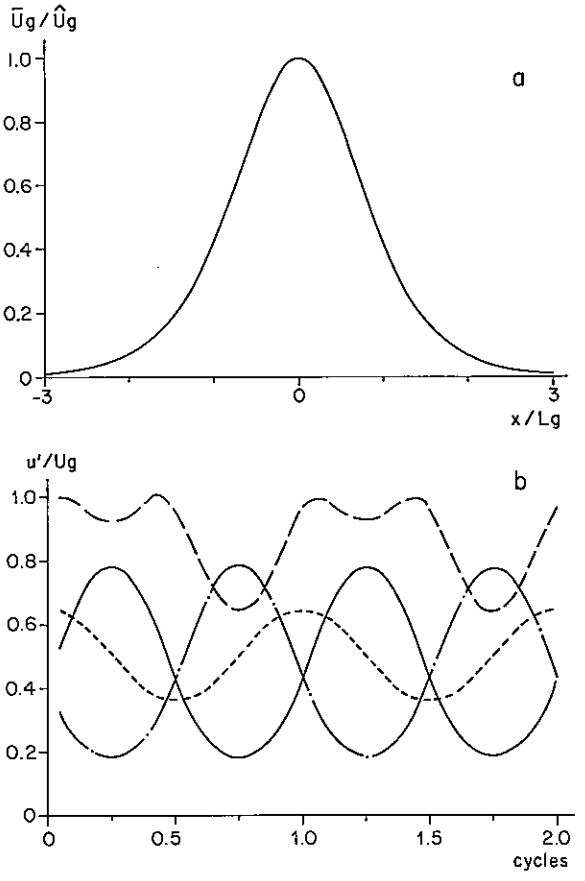

Fig. 8. Synthetically constructed u' (non-dimensionalized by $U_g = \hat{U}_g \sin\alpha$) due to tidal advection of a geostrophical current $\vec{u_g}$ and its dependence on the ratios L_e/L_g and x/L_g (according to (2)). (L_g: typical width of geostrophic current; L_e: tidal excursion length; x: distance of mooring from maximum geostrophic current). Assuming a "$\cosh^{-2}$"-shape in space of $\overline{U_g}$ (a), some special cases are shown in (b): (····) represents the advecting tidal current; (——): $x/L_g = 1$, $L_e/L_g = .5$; (— · —): $x/L_g = -1$; $L_e/L_g = .5$; (- - -): $x/L_g = .2$, $L_e/L_g = .5$. Note that the amplitude of u_0 is not properly scaled.

is acquired when $x/L_e << 1$. The model gives for the relationship between u' and v': $|v'| / |u'| = \cos\alpha/\sin\alpha$, while the phase difference is 0°, independent of z. This should be contrasted with the relationship shown in Table 5 for the case when the fluctuating signals are due to internal tides.

With a barotropic current velocity amplitude of $U_0 = 0.3\ m \cdot s^{-1}$ and, from Fig. 3d, a mean horizontal temperature gradient of $1°C \cdot km^{-1}$, a fluctuating temperature amplitude of 2.1 °C is calculated from (1). This result, which compares

well with estimates from Fig. 2a at 27 m depth, is extended by performing a simple simulation. To perform this simulation, we advect the temperature field in Fig. 2 with the local barotropic current at 30 m depth after interpreting Fig. 2a as a spatial structure by assuming a steady frontal advection speed of 2 cm·s^{-1} in a north-westerly direction. The presence of such an advecting current is suggested by successive hydrographic surveys (like Fig. 3) and this magnitude is close to the observed mean value of the low passed current speed in the lower portion of the water column in this north-westerly direction. The semidiurnally bandpass filtered result of this simulation is shown in Fig. 9. The agreement with Fig. 6a is reasonable at 27, 29 and 31 m depth, so that we can conclude that T′ at these depths may have been caused by frontal advection. An "upper layer front", suggested by Fig. 2a and which consequently shows up in Fig. 9, is not apparent in Fig. 6a. We conclude that this "upper layer front" represents an evolution in time only, and not in space as is also suggested by VAN AKEN *et al.* (1987).

If frontal advection is the cause of T′ a phase difference of 90° between u_0 at 30 m and T′ must be found. The results in Table 4a differ by 25° from this theoretical prediction, which may be due to vertical phase shift of the barotropic current at the lower boundary of the thermocline, found to be around 20° by MAAS & VAN HAREN (1987). A suitable explanation for the observed larger phase differences between u_0 and T′ at station L has not been found.

Some evidence for current fluctuations due to the advection of the geostrophic current can be found in Table 4f. The result around day 237, when u′ lags u_0 by around 95°, is approximately in accordance with a theoretical prediction of 90° when the geostrophic current is assumed to lie west of the moorings (Figs 2, 3 and 9). Using an amplitude of $u' = 7$ cm·s^{-1} (Fig. 7a), the bell-shaped profile for $\overline{U_g}$, $\hat{U}_g = 15$ cm·s^{-1}, $\alpha = 33°$ (Fig. 2b) and $L_e = 2.1$ km, the typical width of the geostrophic current is estimated from (2) to be $L_g = 5.3$ km or about 2.5 times L_e.

However, no further evidence for this type of frontal advection can be found in Table 4f, while the phase difference of 75° between u′ and v′ (Table 4g) is not predicted by the advective model which gives 0°. Probably frictional effects, not considered in (2), are responsible for this deviation. As the vertical current profile of u_0 is a function of depth due to friction, tidal advection will not be rigid, but will cause the dynamical system to be disturbed. Consequently, a geostrophic adjustment process will occur with (super) inertial oscillations causing a phase difference of 90° between u′ and v′.

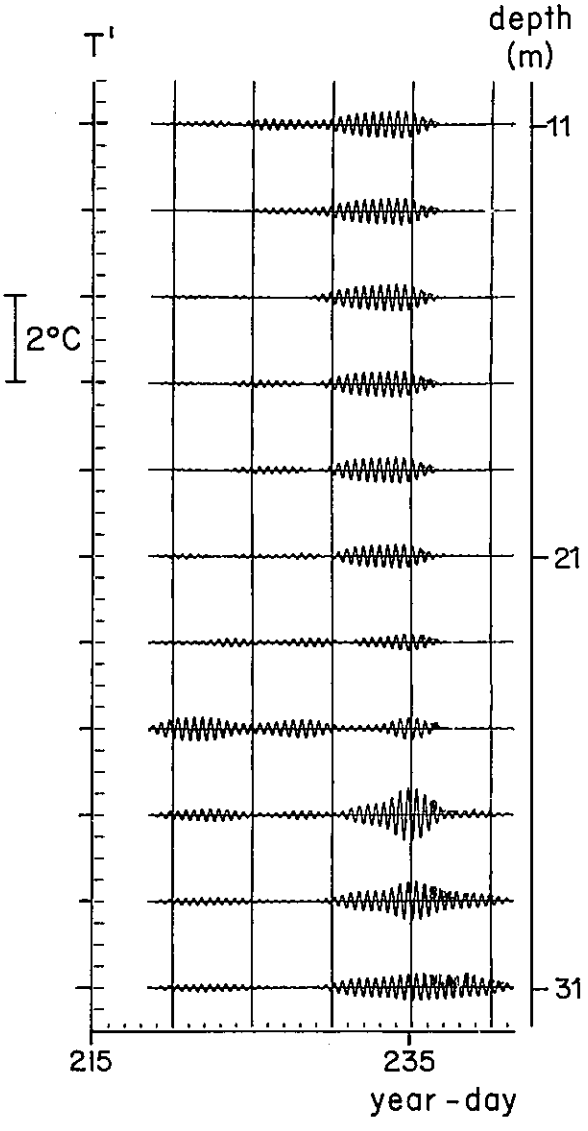

Fig. 9. Bandpass filtered time series of simulated fluctuating temperature signals. The temporal low-pass filtered temperature field was interpreted as a spatially varying field adopting an unidirectional north-westerly displacement speed of 2 cm·s^{-1}, suggested by the passage times of the frontal zone at the moorings.

4.3. PHASE DIFFERENCES IN THE HORIZONTAL PLANE FOR u'

If u_0 causes the existence of u', due to rigid tidal advection of a frontal zone, phase differences between u' in the horizontal plane are expected to be similar to those of u_0. Indeed, the correlation results for u' in the horizontal plane are remarkably good as Table 4e shows significance for nearly every calculation performed. However, the phase differences in Table 4e are an order of magnitude larger than the phase differences over the mooring positions of u_0 of 2 to 3° (Table 2), which are determined for the total time span from harmonic analysis.

Based on a model describing the influence of friction and stratification on the vertical (phase) structure of u_0, an explanation for the observed horizontal phase differences in u' will be described. The underlying assumption is that as stratification is changing through the course of the measurements both in time (Fig. 2a) and in space (Fig. 3) and as different stratification types cause different vertical phase structures of u_0 (MAAS & VAN HAREN, 1987), these changing phase differences consequently are contained in u'. It must be remembered that expected horizontal phase differences for u', identified with internal tides, are in the range of 90°-180°, an order of magnitude larger than those of Table 4e.

The results of Table 4e are plotted in Fig. 10, where they are separated in three classes with similar qualitative features a, b and c. Both near the surface and near the bottom all mooring positions lag position I in phase for class a (the stratified period), with a maximum phase lag of about 40° between I and L around day 223. Classes b and c describe horizontal phase differences near the surface and near the bottom, respectively, during the periods of the frontal passage (around day 237) and well-mixed waters (around day 245). Class b shows a maximum phase difference of 15° to 20° between L and J (J lagging L). For class c, especially during the frontal passage, small horizontal phase differences occur.

Horizontal phase differences, measured during the frontal passage (classes b and c), cannot be explained by rigid advection of a geostrophic current jet, since this will result in horizontal phase differences of 0° or 180°, depending on the mooring positions in relation to the jet's maximum. A possible explanation for the phase differences of classes b and c will be given by using

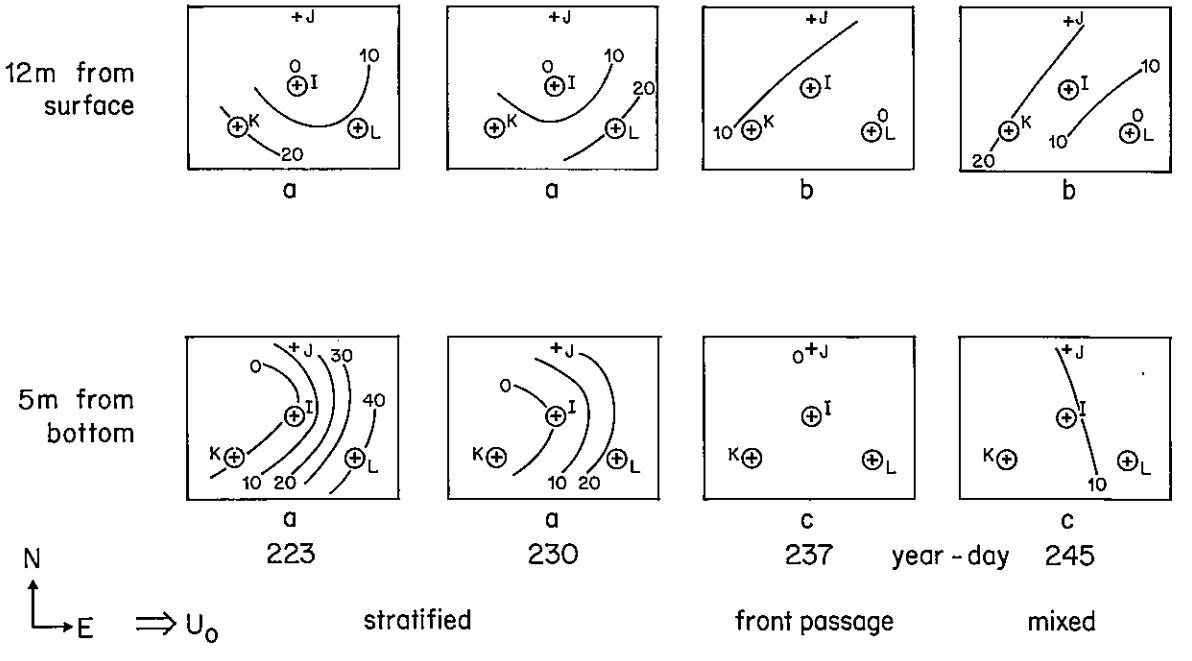

Fig. 10. Phase differences in degrees between u' at different positions in the horizontal plane near the surface and the bottom (Table 4e). Different classes explained in the text are denoted by a, b and c. The double arrow shows the barotropic tidal current direction.

Fig. 11, where vertical phase profiles for u_0 are related to the stratification depth. Curves a and c are theoretical best-fit curves to measurements (•), which show different vertical phase profiles in stratified and well-mixed waters, while the vertical phase differences between the current meters near the bottom and near the surface have the same value of 23° (MAAS & VAN HAREN, 1987).

The model used by MAAS & VAN HAREN (1987) consisted of three layers in which Ekman dynamics were applied. The middle layer, representing the thermocline, was centered around mid-depth, leaving its thickness as a variable parameter. Two other variable parameters described the eddy viscosities of the surface and bottom layers, which were given the same value E_1, and of the middle layer (E_2), with $E_2 << E_1$ because of the stabilizing effect of stratification. All solutions of the model were matched at the boundaries yielding a fourth variable parameter describing the bottom stress. By varying the parameters a description, in terms of Ekman dynamics, of the vertical structure of barotropic currents was found by fitting the model curves to the measurements. This model is here extended to calculate vertical profiles in a frontal zone, simply by introducing a variable parameter for the mean depth of the thermocline. Curve b, calculated for a mean thermocline depth of z/H = 0.23, shows an enhanced vertical phase difference for u_0 of 38°.

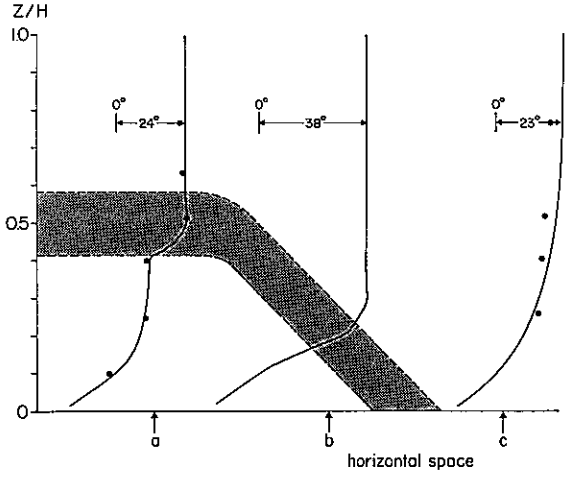

Fig. 11. Theoretical (——) and observed (•) vertical phase profiles for u_0 for three different thermocline depths denoted by a, b and c in space (after MAAS & VAN HAREN, 1987). The position of the thermocline is shaded. The phase differences between the current meters near the surface and near the bottom are given for each profile.

Comparing curve b with curves a or c, we may expect horizontal phase differences of 15° (0°) for u_0 near the surface (bottom) due to a different vertical momentum transfer within the frontal zone. As Fig. 11 shows, different vertical phase differences in the barotropic current occur at different positions and times, depending on the position or time of passage of a frontal zone. As the barotropic currents are determined from harmonic series spanning the total period of measurement, of which the time of frontal passage took only some 10%, due to the migration in north-west direction of the frontal zone, these changing vertical phase differences are assumed to be averaged out in the barotropic currents. They should consequently be contained in u'. Note that in this interpretation no u' would have been detected if the stratification was stationary at the mooring positions.

No suitable explanation has been found for the phase differences of class a.

5. CONCLUSIONS

Although a strong stratification was present during the period of measurement in a continental shelf sea, difficulties in identifying internal tides in shallow seas have been brought to light (*cf.* WUNSCH, 1975). Even in temperature signals hardly any evidence for internal tides was found by comparing phases at different moorings. One of the main causes of the fluctuating signals u' and T' is associated with the presence of a frontal zone close to the moorings. At least during the passage of this front along the mooring positions, fluctuating temperature and velocity signals seemed to be due to tidal advection of the frontal zone. The observed horizontal phase differences of 20° in the fluctuating current signals may be due to a phase shift of the barotropic tide associated with a spatial change in thermocline depth.

6. REFERENCES

AKEN VAN, H.M., 1983. Project "gelaagde Noordzee 81/82" CTD waarnemingen 1982. Internal report IMO-Utrecht V83-18 (unpublished).

AKEN VAN, H.M., G.J.F. VAN HEIJST & L.R.M. MAAS, 1987. Observations of fronts in the North Sea. (to be publ. in J. mar. Res.).

BAINES, P.G., 1982. On internal tide generation models.—Deep Sea Res. **29**: 307-338.

DRONKERS, J.J., 1964. Tidal computations in rivers and coastal waters. North Holland Publishing Company, Amsterdam: 1-518.

HOLLOWAY, P.E., 1983. Internal tides on the Australian North-West shelf: a preliminary investigation.—J. Phys. Oceanogr. **13:** 1357-1370.

JONES, I.S.F. & L. PADMAN, 1983. Semidiurnal internal tides in Eastern Bass Strait.—Aust. J. mar. Freshw. Res. **34:** 159-171.

KOBLINSKY, C.J., 1981. The M_2 tide on the West Florida Shelf.—Deep Sea Res. **28A:** 1517-1532.

LEBLOND, P.H. & L.A. MYSAK, 1978. Waves in the ocean. Elsevier, Amsterdam: 1-602 pp.

MAAS, L. & H. VAN HAREN, 1986. Data report of current, temperature and pressure observations. Stratified Central North Sea 1980-1982. IMO-Utrecht Report R-86-14 (unpublished).

MAAS, L.R.M. & J.J.M. VAN HAREN, 1987. Observations on the vertical structure of tidal and inertial currents in the Central North Sea.—J. mar. Res. **45:** (in press).

MARTINSEN, E.A. & J.A. WEBER, 1981. Frictional influence on internal Kelvin waves.—Tellus, **33:** 402-410.

MUIR, L.R., 1980. Internal tides in a partially-mixed estuary. In: T. Carstens & T. McClimans. Second international symposium on stratified flows. —Trondheim, **1:** 538-547.

PETRIE, B., 1975. M_2 surface and internal tides on the Scotian shelf and slope.—J. mar. Res. **33:** 303-323.

SCHOTT, F., 1971. On horizontal coherence and internal wave propagation in the North Sea.—Deep Sea Res. **18:** 291-307.

——, 1977. On the energetics of baroclinic tides in the North Atlantic.—Ann. Geophys. **33:** 41-62.

SHERWIN, T.J., 1987. The internal tide on the Malin Shelf. Preprints of the proceedings of the 3rdInternational Symposium on Stratified Flows, Pasadena California.

TEE, K.-T., 1982. The structure of three-dimensional tide-generating currents: experimental verification of a theoretical model.—Estuar. coast. Shelf Sci. **14:** 27-48.

THOMPSON, R.O.R.Y., 1979. Coherence significance levels.—J. Atmos. Sci. **36:** 2020-2021.

WUNSCH, C., 1975. Internal tides.—Rev. Geophys. Space Phys. **13:** 167- 182.

(received 15-1-1987; revised 13-4-1987)